Electronic Supplementary Material (ESI) for Journal of Materials Chemistry A.

Supplementary Information

Synthesis of Yolk-Shell $Co_3O_4/Co_{1-x}Ru_xO_2$ Microspheres Featuring an Enhanced Electrocatalytic Oxygen Evolution in Acidic Medium

Abinaya Annamalai,[a,d] Dipak V.Shinde,[a*] Joka Buha,[a] Sergio Marras,[b] Mirko Prato,[b] Simone Lauciello,[c] Luca De Trizio[a*] and Liberato Manna [a*]

[a]Nanochemistry Department, [b]Materials Characterization Facility, [c]Electron Microscopy Facility, Istituto Italiano di Tecnologia, via Morego 30, 16163 Genova, Italy.

[d]Dipartimento di Chimica e Chimica Industriale, Università degli Studi di Genova, Via Dodecaneso, 31, Genova, Italy.

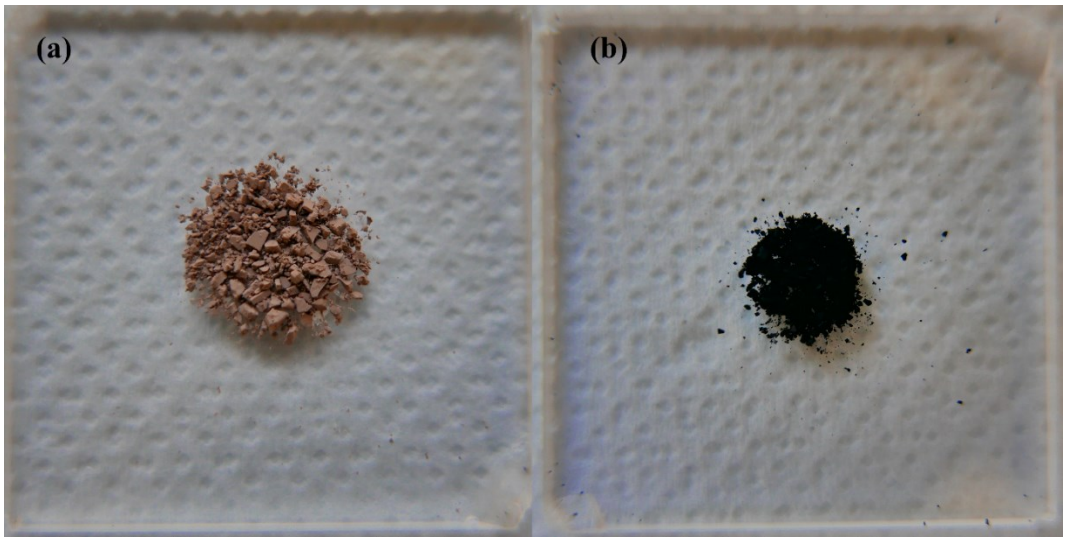

Figure S1. Photographs of (a) Cobalt glycerate (Co-G) and (b) yolk-shell $Co_3O_4/Co_{1-x}Ru_xO_2$ MSs.

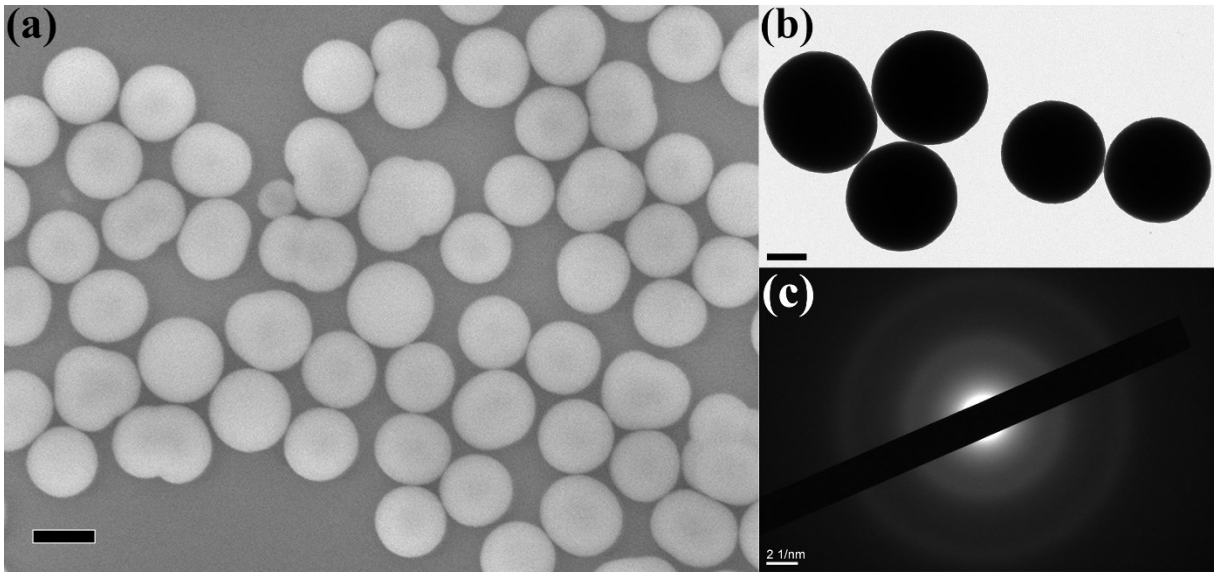

Figure S2. (a) FESEM image (Scale bar: 500 nm) and (b) TEM image (Scale bar: 200 nm) of Co-G spheres and its corresponding (c) SAED pattern (Scale bar: 2 1/nm) indicating that the spheres are amorphous.

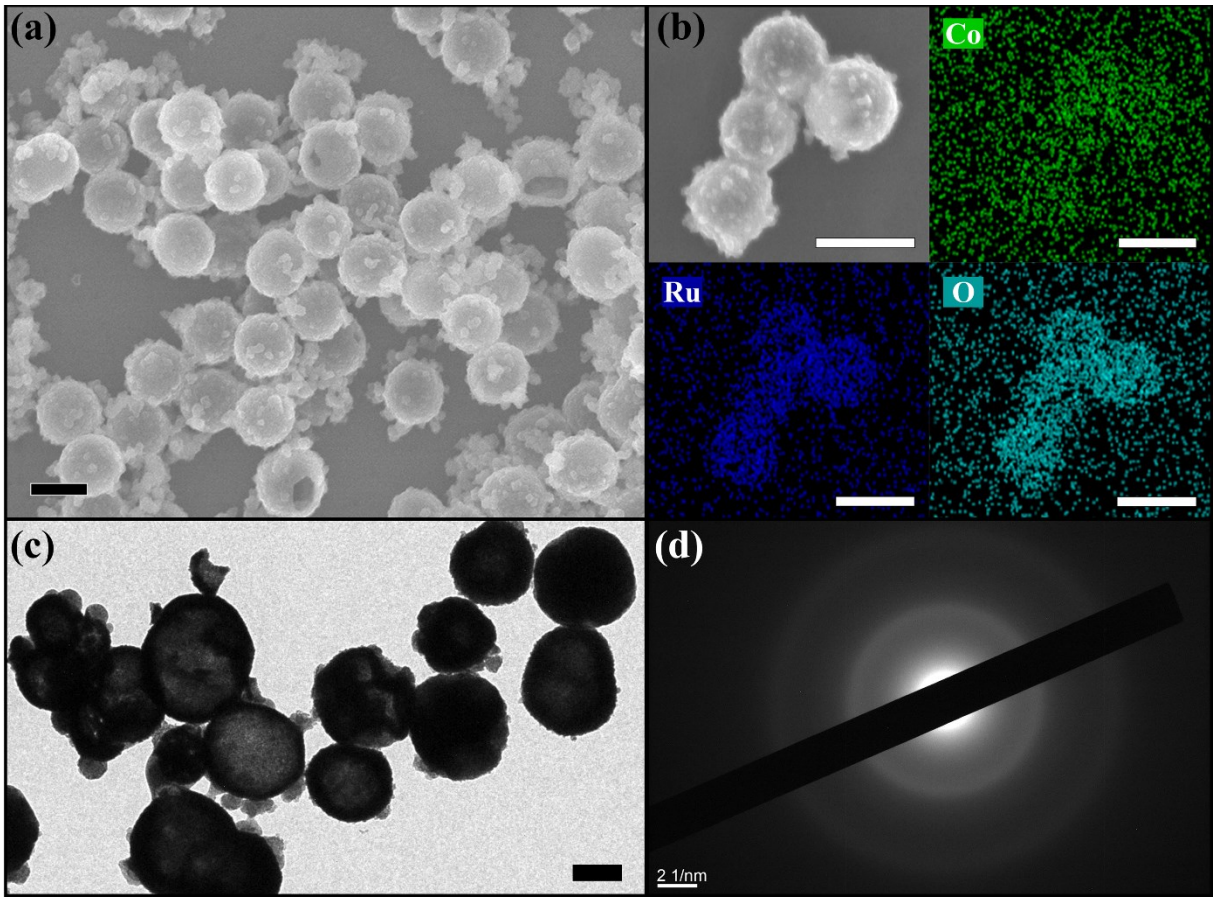

Figure S3. (a) FESEM image of the product obtained by reacting Co-G with $RuCl_3$ (Co-Ru oxide Precursor) (Scale bar: 500 nm). (b) An FESEM image and the corresponding EDX mapping of Co-Ru precursor with Co, Ru and O elemental maps (Scale bars: 500 nm). (c) TEM image (scale bar: 200 nm) and the corresponding (d) SAED pattern (Scale bar: 2 1/nm) of Co-Ru indicating that the material is still amorphous.

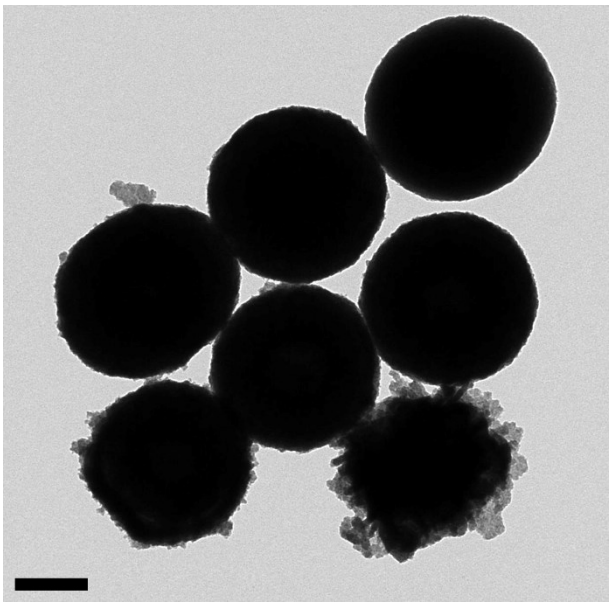

Figure S4. TEM image Co-Ru oxide precursor produced by reacting insufficient amount of $RuCl_3$ (30 ml of a 1mg/ml $RuCl_3$ solution in this case) with Co-G which left many Co-G spheres bare or poorly covered with RuO_2 (Scale bar: 100 nm).

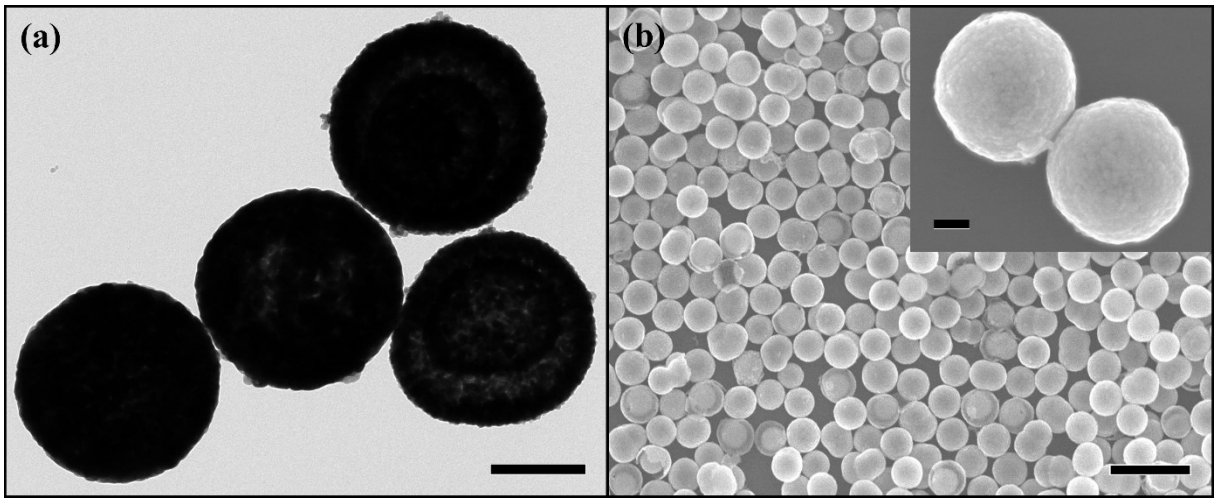

Figure S5. (a) TEM (scale bar: 200 nm) and (b) FESEM (scale bar: 1 μm) images of Co_3O_4 spheres. Inset: An enlarged image of Co_3O_4 spheres (scale bar: 100 nm). The Co_3O_4 spheres were prepared by annealing the as synthesized Co-G powder (Figure S2) at 350^0C for 1 hour using a muffle furnace @ 2^0C/min under air atmosphere.

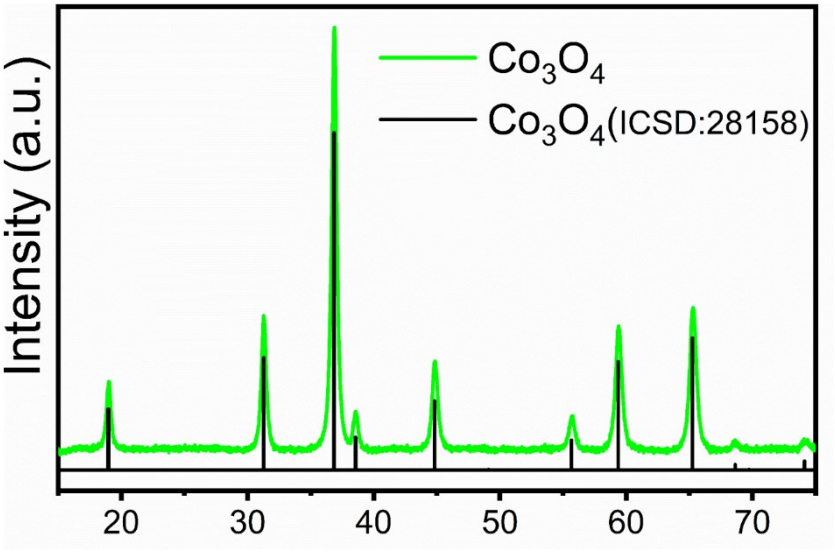

Figure S6. XRD pattern of as-synthesized pristine hollow Co_3O_4 spheres and the matching reference pattern ICSD 28158.

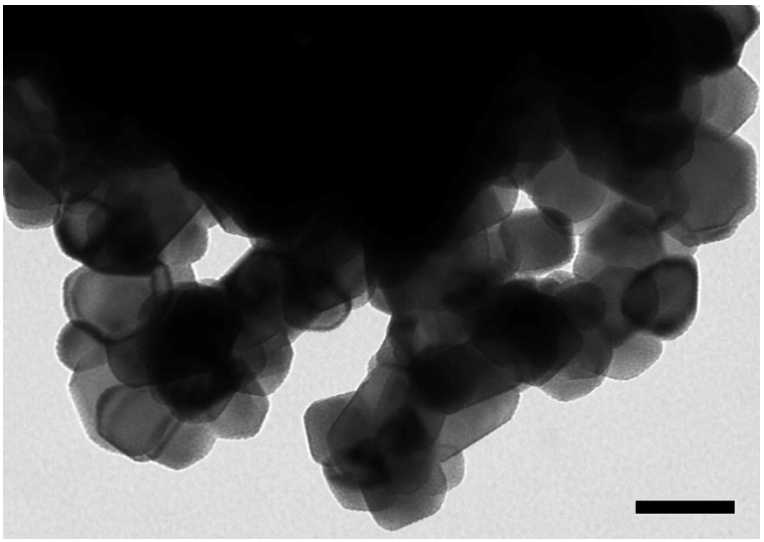

Figure S7. TEM image of the commercial RuO_2 nanoparticles. Scale bar: 50 nm.

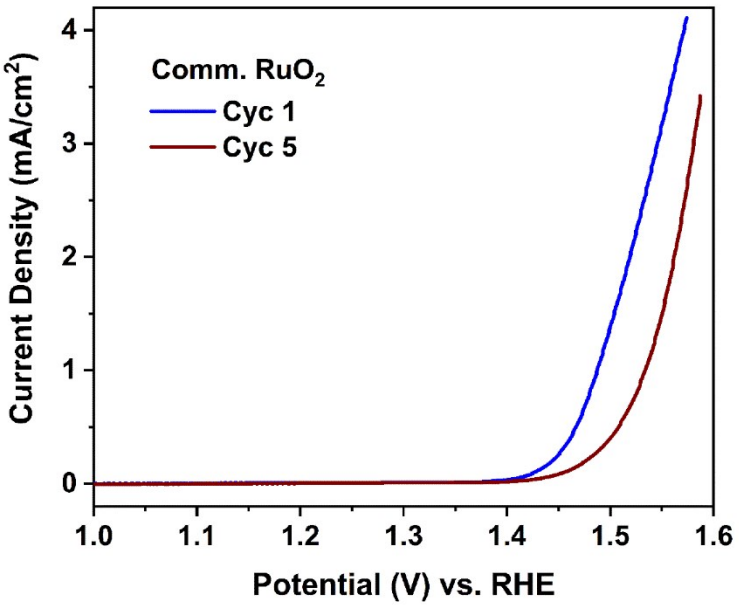

Figure S8. LSV of commercial RuO_2 at its first and fifth cycle.

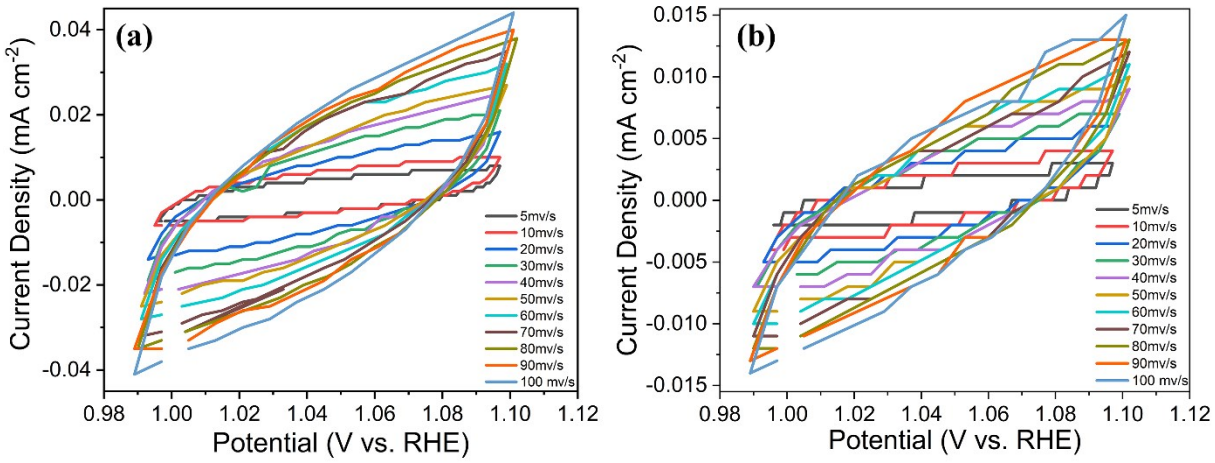

Figure S9. Measurement of the double layer capacitance of MSs. (a) CVs of MSs annealed at 350^0C and (b) RuO_2, collected at various scan rates.

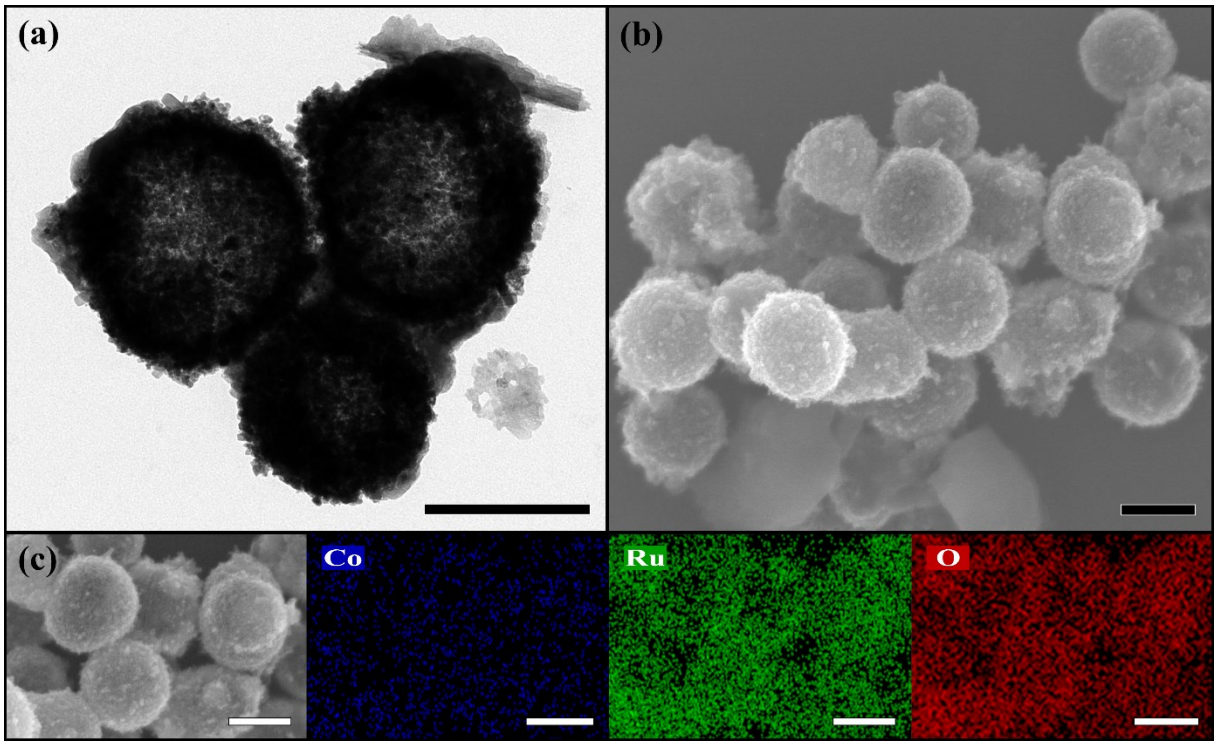

Figure S10. (a) TEM, (b) FESEM image of MSs after 24 h of chronopotentiometry measurement. (c) The corresponding FESEM image and EDX elemental mapping of Co, Ru and O. (Scale bars: 250 nm).

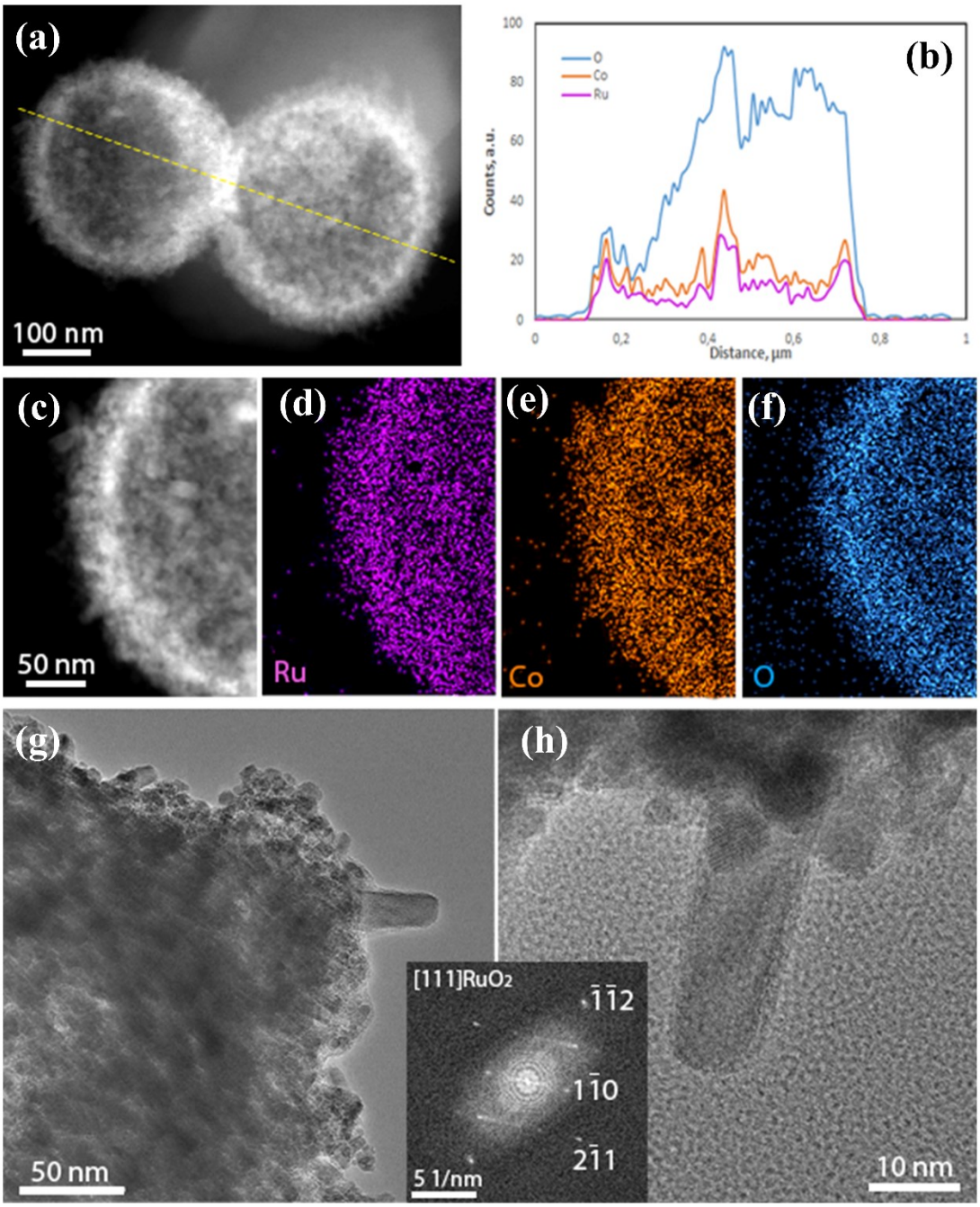

Figure S11. (a) HAADF-STEM image of yolk-shell MSs with the corresponding (b) EDX elemental line profile across the middle of the spheres after 24 h of chronopotentiometry measurement. (c) HAADF-STEM image and the corresponding (d-f) EDX elemental mapping showing the distribution of Co, Ru and O. (g,h) HRTEM images of the surface of one of the MSs showing the nanorods. Inset: FFT from one of the nanorods indexed according to RuO_2 tetragonal structure.

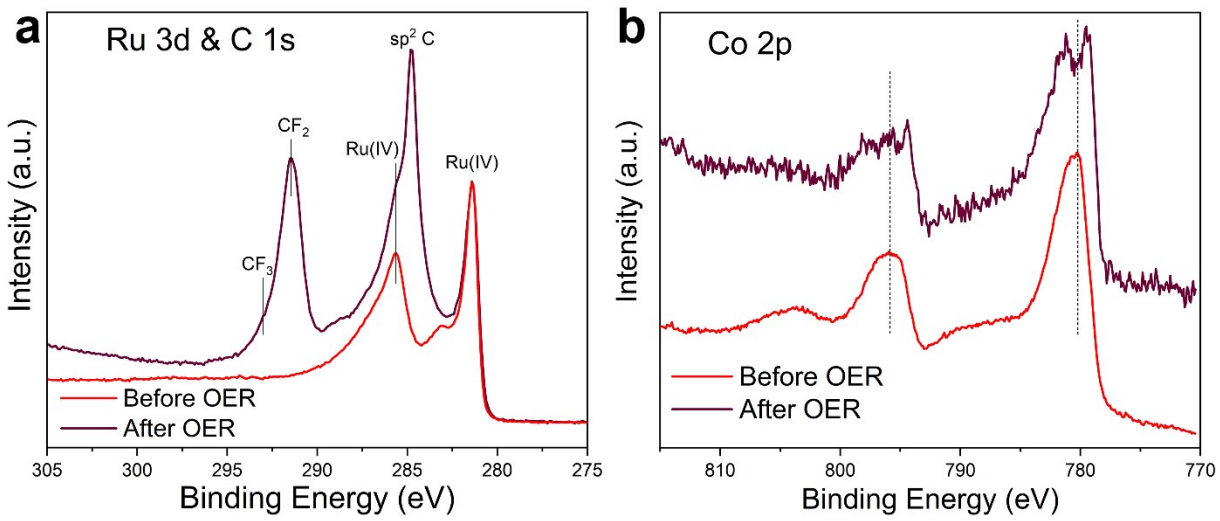

Figure S12. High-resolution XPS spectra collected on the energy ranges typical for (a) Ru 3d and (b) Co 2P peaks before and after 24 h of chronopotentiometry measurement @ 10mA cm^{-2}.

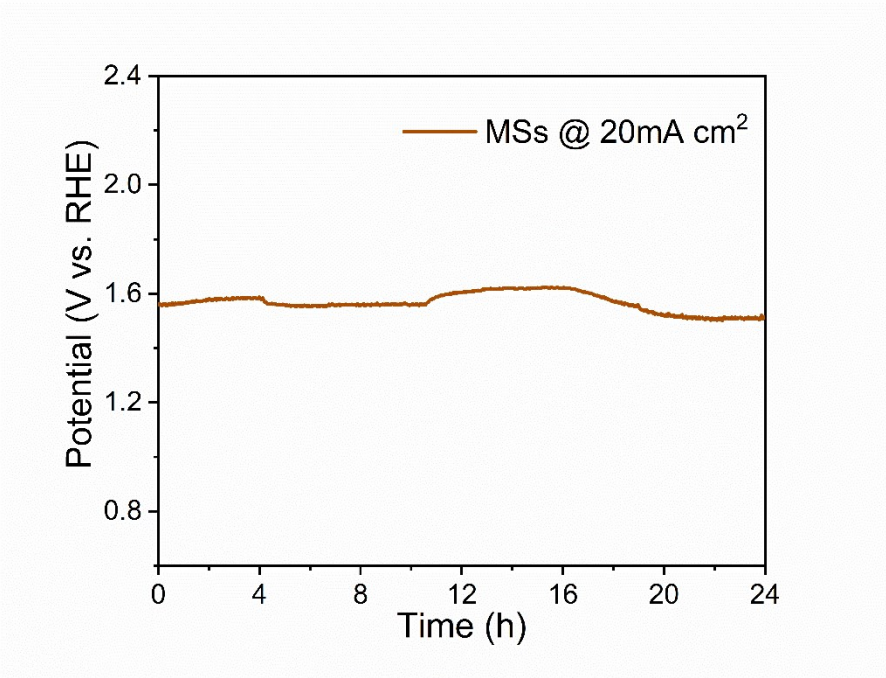

Figure S13. Chronopotentiometry curve under constant current density of 20 mA cm^{-2}

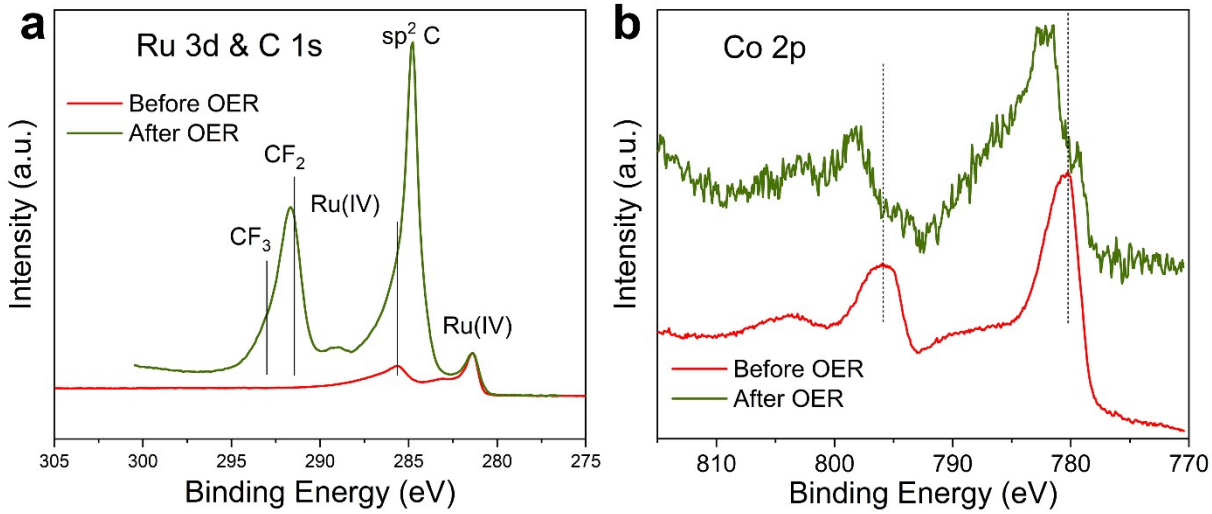

Figure S14. High-resolution XPS spectra collected at the energy ranges typical for (a) Ru 3d and (b) Co 2p peaks before and after 24 h of chronopotentiometry measurement @ 20mA cm^{-2}.

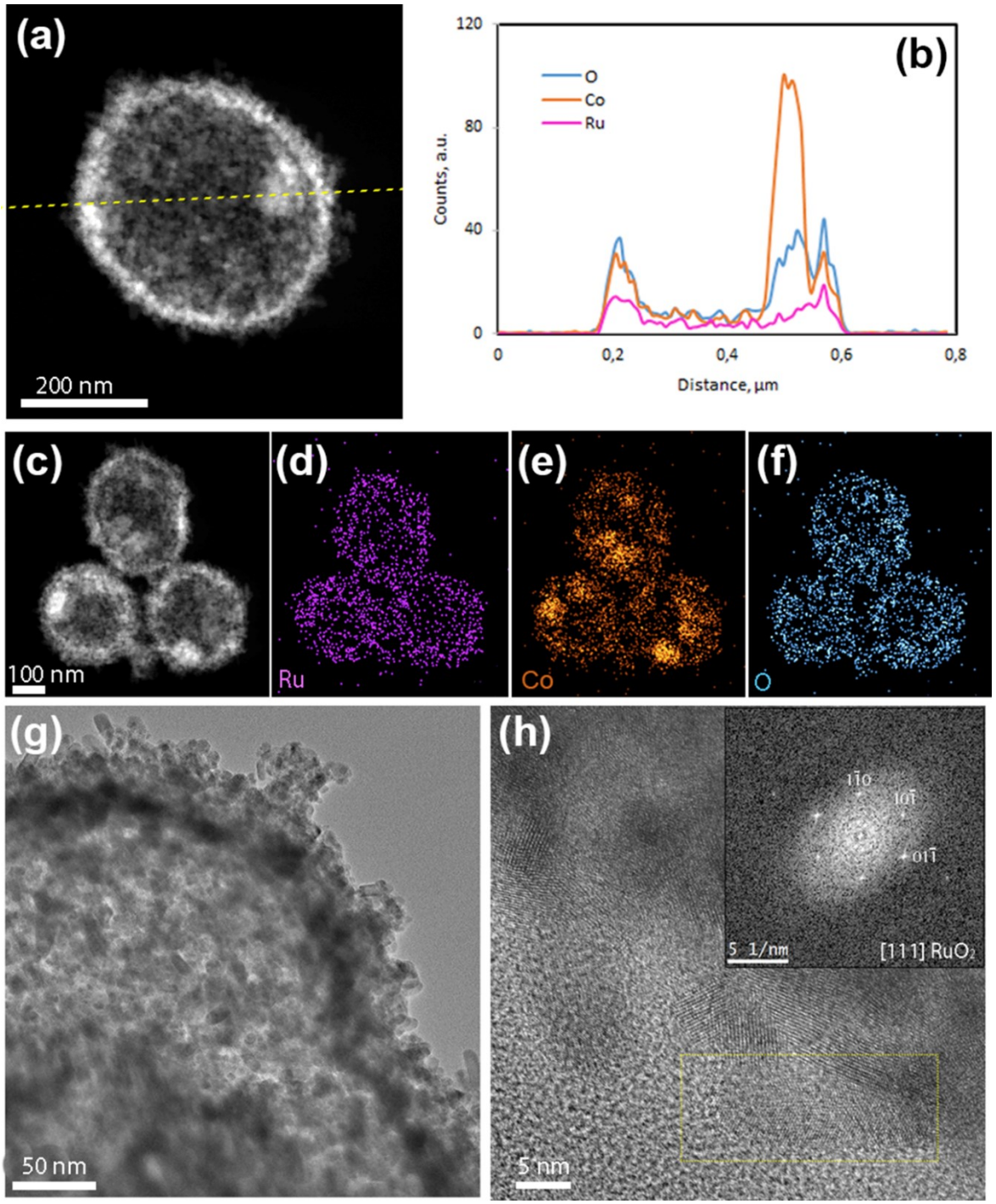

Figure S15. (a) HAADF-STEM image of yolk-shell MSs with the corresponding (b) EDX elemental line profile across the middle of the spheres after 24 h of chronopotentiometry measurement @20mA cm^{-2}. (c) HAADF-STEM image and the corresponding (d-f) EDX elemental mapping showing the distribution of Co, Ru and O. (g,h) HRTEM images of the surface of one of the MSs showing the nanorods. Inset of (h) is the FFT from one of the nanorods (that in the orange rectangle) indexed according to the RuO_2 tetragonal structure.

Supplementary Table S1. The comparison of overpotential with other reported OER electrocatalysts in acidic media.

Catalyst	Electrolyte	Overpotential at 10 mA cm^{-2} (mV)	Stability at specific current density	Ref.
$Co_3O_4/Co_{1-x}Ru_xO_2$ MSs	0.5 M H_2SO_4	240@10 mA cm^{-2} 170@1mA cm^{-2}	24 h @10 mA cm^{-2}	This Work
$IrO_x/SrIrO_3$	0.5 M H_2SO_4	270-290	30 h @10 mA cm^{-2}	1
$Ru@IrO_x$	0.05 M H_2SO_4	282	24 h @10 mA cm^{-2}	2
$Ir_{0.5}W_{0.5}@NC$	0.5 M H_2SO_4	270	8 h @10 mA cm^{-2}	3
$RuO_2@Ru/RuO_2$	0.5 M H_2SO_4	219	8 h @10 mA cm^{-2}	4
$IrCo_x$	0.1 M $HClO_4$	300	14 h @10 mA cm^{-2}	5
Ir NP	0.5 M H_2SO_4	320	10 h @10 mA cm^{-2}	6
IrNiCu HCSA	0.5 M H_2SO_4	300	20 h @10 mA cm^{-2}	7
IrO_x–$Ni(OH)_2$	0.1 M $HClO_4$	350	2 h @10 mA cm^{-2}	8
IrRu@Te	0.5 M H_2SO_4	220	10 h @10 mA cm^{-2}	9
$RuO_2@IrO_2$	0.5 M H_2SO_4	250	1 h @200 mA cm^{-2}	10
$Cr_{0.6}Ru_{0.4}O_2$	0.5 M H_2SO_4	178	10 h @10 mA cm^{-2}	11
$Y_2Ru_2O_{7-\delta}$	0.1 M $HClO_4$	270@1 mA cm^{-2}	8 h@1 mA cm^{-2}	12
$BaYIrO_6$	0.1 M $HClO_4$	315	1 h@10 mA cm^{-2}	13
IrO_2-RuO_2 @Ru	0.5 M H_2SO_4	281	--	14
RuRh@$(RuRh)O_2$ NSs/C	0.1 M $HClO_4$	245	2.2 h @5 mA cm^{-2}	15
IrNiCu DNF/C	0.1 M $HClO_4$	300	--	16

References

1. L. C. Seitz, C. F. Dickens, K. Nishio, Y. Hikita, J. Montoya, A. Doyle, C. Kirk, A. Vojvodic, H. Y. Hwang and J. K. Norskov, *Science*, 2016, **353**, 1011-1014.
2. J. Shan, C. Guo, Y. Zhu, S. Chen, L. Song, M. Jaroniec, Y. Zheng and S.-Z. Qiao, *Chem*, 2019, **5**, 445-459.
3. K. Fan, M. He, N. A. Dharanipragada, P. Kuang, Y. Jia, L. Fan, A. K. Inge, B. Zhang, L. Sun and J. Yu, *Sustain. Energy Fuels*, 2020, **4**, 1712-1722.
4. Z. Wang, B. Xiao, Z. Lin, S. Shen, A. Xu, Z. Du, Y. Chen and W. Zhong, *J. Energy Chem.*, 2021, **54**, 510-518.
5. W. Gao, Q. Xu, Z. Wang, M. Wang, X. Ren, G. Yuan and Q. Wang, *Electrochim. Acta*, 2020, **337**, 135738.
6. J. A. Arminio-Ravelo, J. Quinson, M. A. Pedersen, J. J. Kirkensgaard, M. Arenz and M. Escudero-Escribano, *ChemCatChem*, 2020, **12**, 1282-1287.
7. J. Zhang, Z. Chen, C. Liu, J. Zhao, S. Liu, D. Rao, A. Nie, Y. Chen, Y. Deng and W. Hu, *Sci. China Mater.*, 2020, **63**, 249-257.
8. J. Ruiz Esquius, G. Algara-Siller, I. Spanos, S. J. Freakley, R. Schlögl and G. J. Hutchings, *ACS Catal.*, 2020, **10**, 14640-14648.
9. J. Xu, Z. Lian, B. Wei, Y. Li, O. Bondarchuk, N. Zhang, Z. Yu, A. Araujo, I. Amorim and Z. Wang, *ACS Catal.*, 2020.
10. Z. Ma, Y. Zhang, S. Liu, W. Xu, L. Wu, Y.-C. Hsieh, P. Liu, Y. Zhu, K. Sasaki and J. N. Renner, *J. Electroanal. Chem.*, 2018, **819**, 296-305.
11. Y. Lin, Z. Tian, L. Zhang, J. Ma, Z. Jiang, B. J. Deibert, R. Ge and L. Chen, *Nat. Commun.*, 2019, **10**, 1-13.
12. J. Kim, P.-C. Shih, K.-C. Tsao, Y.-T. Pan, X. Yin, C.-J. Sun and H. Yang, *J. Am. Chem. Soc.*, 2017, **139**, 12076-12083.
13. O. Diaz-Morales, S. Raaijman, R. Kortlever, P. J. Kooyman, T. Wezendonk, J. Gascon, W. Fu and M. T. Koper, *Nat. Commun.*, 2016, **7**, 1-6.
14. G. Li, S. Li, J. Ge, C. Liu and W. Xing, *J. Mater. Chem.*, 2017, **5**, 17221-17229.
15. K. Wang, B. Huang, W. Zhang, F. Lv, Y. Xing, W. Zhang, J. Zhou, W. Yang, F. Lin, P. Zhou, M. Li, P. Gao and S. Guo, *J. Mater. Chem.*, 2020, **8**, 15746-15751.
16. J. Park, Y. J. Sa, H. Baik, T. Kwon, S. H. Joo and K. Lee, *ACS Nano*, 2017, **11**, 5500-5509.